CELL BIOLOGY

The Suv420h histone methyltransferases regulate PPAR-γ and energy expenditure in response to environmental stimuli

Simona Pedrotti[1], Roberta Caccia[1]*, Maria Victoria Neguembor[1]*†, Jose Manuel Garcia-Manteiga[2], Giulia Ferri[1], Clara de Palma[3], Tamara Canu[4], Matteo Giovarelli[5], Paolo Marra[4], Amleto Fiocchi[6], Ivan Molineris[2], Michele Raso[6], Francesca Sanvito[7], Claudio Doglioni[7], Antonio Esposito[4], Emilio Clementi[5,8], Davide Gabellini[1]‡

Obesity and its associated metabolic abnormalities have become a global emergency with considerable morbidity and mortality. Epidemiologic and animal model data suggest an epigenetic contribution to obesity. Nevertheless, the cellular and molecular mechanisms through which epigenetics contributes to the development of obesity remain to be elucidated. Suv420h1 and Suv420h2 are histone methyltransferases responsible for chromatin compaction and gene repression. Through in vivo, ex vivo, and in vitro studies, we found that Suv420h1 and Suv420h2 respond to environmental stimuli and regulate metabolism by down-regulating peroxisome proliferator–activated receptor gamma (PPAR-γ), a master transcriptional regulator of lipid storage and glucose metabolism. Accordingly, mice lacking Suv420h proteins activate PPAR-γ target genes in brown adipose tissue to increase mitochondria respiration, improve glucose tolerance, and reduce adipose tissue to fight obesity. We conclude that Suv420h proteins are key epigenetic regulators of PPAR-γ and the pathways controlling metabolism and weight balance in response to environmental stimuli.

INTRODUCTION

Obesity is a pandemic disorder with serious health concerns for affected individuals (*1*), raising the risks of diabetes, hypertension, atherosclerosis, and cancer (*2*). Since obesity develops when energy intake exceeds energy expenditure (*1*), current therapeutic strategies aim at restricting energy uptake and absorption. However, these approaches show limited efficacy and alternative strategies are urgently needed to increase energy dissipation.

Obesity, diabetes, and metabolic diseases are complex disorders with only partial genetic heritability, indicating important roles for environmental programming and epigenetic effects (*3*). It has been argued that the epigenome may represent the mechanistic link between genetic variants and environmental factors in determining the obesity risk (*3*).

Adipose tissue is critical for the maintenance of metabolic homeostasis through its effects on energy balance and its endocrine function. It fulfills important roles in whole-body lipid handling, serves as the body's major energy storage compartment, and secretes numerous endocrine mediators (*4*). The adipose organ can be divided into two main types of adipose tissues, white adipose tissue (WAT) and brown adipose tissue (BAT). While WAT mainly stores energy and is increased in obesity, BAT dissipates energy by generating heat through non-shivering thermogenesis. This activity is allowed via specific expression of uncoupling protein 1 (Ucp1), which diminishes the proton gradient by uncoupling cellular respiration and mitochondrial adenosine triphosphate synthesis (*5*). Adult humans have active BAT deposits (*6*), which display substantial metabolic activity also during warm conditions when thermogenesis is not required (*7*). Moreover, very recently, it was shown that a meal elevates human BAT glucose uptake and thermogenesis to the same extent as cold stress (*7*). The amount of BAT inversely correlates with adiposity and body mass index in humans (*6*). In addition to "classic BAT," various environmental stimuli including cold exposure (*8*) induce the emergence of brown adipocyte-like cells (beige/brite adipocytes) within WAT. Activated human brown/beige fat improves whole-body glucose homeostasis and insulin sensitivity and can lead to reduced body weight (*9*), indicating that it plays an important role in energy homeostasis in adult humans. Hence, a better understanding of the molecular control of BAT function may allow one to address of obesity and metabolic disorders (*9*).

Peroxisome proliferator–activated receptor gamma (PPAR-γ) is highly expressed in BAT and is a master transcriptional regulator of glycemic metabolism, adipogenesis, energy balance, and lipid biosynthesis (*10*, *11*). PPAR-γ displays decreased expression in obese subjects with diabetes. Moreover, dominant negative mutations in PPAR-γ are associated with severe insulin resistance, diabetes, and hypertension (*12*, *13*). Thiazolidinediones (TZDs), synthetic ligands of PPAR-γ, are the only current antidiabetic agents that function primarily by increasing insulin sensitivity (*14*, *15*). The adipose tissue is the major site of action for the insulin-sensitizing actions of PPAR-γ (*14*). However, despite clear benefits in glycemic control, TZDs have recently fallen into disuse due to concern over side effects and adverse reactions. A number of TZD side effects are PPAR-γ–independent off-target effects (*16*). Notably, recent evidence

[1]IRCCS San Raffaele Scientific Institute, Division of Genetics and Cell Biology, Milano, Italy. [2]IRCCS San Raffaele Scientific Institute, Center for Translational Genomics and BioInformatics, Milano, Italy. [3]Unit of Clinical Pharmacology, University Hospital "L. Sacco"-ASST Fatebenefratelli Sacco, Milano, Italy. [4]IRCCS San Raffaele Scientific Institute, Preclinical Imaging Facility, Milano, Italy. [5]Department of Biomedical and Clinical Sciences "L. Sacco", Università degli Studi di Milano, Milano, Italy. [6]IRCCS San Raffaele Scientific Institute, Mouse Clinic, Milano, Italy. [7]IRCCS San Raffaele Scientific Institute, Division of Experimental Oncology, Milano, Italy. [8]Scientific Institute IRCCS Eugenio Medea, Bosisio Parini, Lecco, Italy.
*These authors contributed equally to this work.
†Present address: Centre for Genomic Regulation (CRG), The Barcelona Institute of Science and Technology, Barcelona, Spain.
‡Corresponding author. Email: gabellini.davide@hsr.it

indicates that a better understanding of PPAR-γ regulation in the adipose tissue could help develop safer and more effective diabetes therapeutics (*17*, *18*).

The histone methyltransferases Suv420h1 (KMT5B) and Suv420h2 (KMT5C) catalyze the di- and trimethylation of lysine 20 in histone H4 (H4K20me2 and H4K20me3), leading to chromatin compaction and gene repression (*19*–*21*). Several studies link Suv420h enzymes to metabolism regulation, suggesting an evolutionarily conserved role in obesity. The human *SUV420H1* gene maps on chromosome 11q13 (*22*) to a 400-kb candidate region for diabetes, and diabetes can be part of the disorders associated to *SUV420H1* mutation (*23*). H4K20me3 is altered in experimental diabetes (*24*) and in a mouse model of Prader-Willi syndrome (*25*, *26*), characterized by obesity in children. H4K20me3 correlates with *Agouti* gene expression, associated with obesity in mice (*27*, *28*). An increase in H4K20me3 at the insulin gene promoter in undernourished rat models correlates with decreased insulin expression and higher susceptibility to streptozotocin-induced diabetes (*29*). The increase in Suv420h2 and H4K20me3 has been linked to the repression of *sod2* and the development and progression of diabetic retinopathy (*24*). In *Caenorhabditis elegans*, Suv420h and H4K20me3 are regulated by the mTORC2 subunit Rictor (*30*), essential for normal BAT growth and lipogenic metabolic state (*31*). Last, Suv420h proteins have been lately implicated in intergenerational metabolic programming in *Drosophila melanogaster*, mice, and humans (*32*). While these results suggest that Suv420h could constitute a nexus between environmental stimuli and metabolism, a direct link between Suv420h epigenetic activity and metabolism is still lacking.

Here, we demonstrate that Suv420h proteins directly inhibit the expression of PPAR-γ and regulate metabolism and body weight. We found that mice lacking Suv420h proteins display a strong PPAR-γ activation signature, increased BAT mitochondria respiration, improved glucose tolerance, reduction in adipose tissue, WAT browning, and resistance to obesity. Collectively, our results promote Suv420h proteins as epigenetic regulators of energy balance that could be targeted for the treatment of obesity.

RESULTS

Suv420h dKO mice display enhanced brown adipocyte metabolic activity

Lineage-tracing studies indicate that early mesenchymal precursor cells expressing the transcription factor Myf5 give rise to muscle cells and brown adipocytes (*33*, *34*). Consequently, several recent studies have used the *Myf5-Cre* knock-in allele to investigate BAT development and function (*33*, *35*–*39*). Because a whole-body knockout (KO) of *Suv420h1* causes lethality and Suv420h1 and Suv420h2 share functional redundancy (*20*), to investigate the role of Suv420h proteins in metabolism regulation, we generated double-KO mice lacking *Suv420h1* and *Suv420h2* in the *Myf5* lineage (henceforth referred to as dKO mice) (fig. S1, A and B). Suv420h1$^{+/+}$, Suv420h$^{+/+}$, and Myf5-Cre were used as controls. No developmental abnormalities were observed in dKO mice compared to controls. We found that only the deletion of both genes resulted in an almost complete absence of H4K20me3 in BAT, while single-KO mice for either Suv420h1 or Suv420h2 showed significant residual levels of the histone mark (fig. S1C), further supporting the redundancy of Suv420h enzymes in BAT.

We observed almost 30% reduction of interscapular BAT (iBAT) mass in dKO mice compared to controls (Fig. 1A), while the weight of other metabolic tissues was not affected (fig. S1D). Accordingly, microscopic analysis on hematoxylin and eosin (H&E)–stained sections revealed that brown adipocytes are smaller in dKO compared to controls (Fig. 1A). Instead, no obvious muscle phenotype was observed in dKO mice (fig. S1, D and E), possibly due to the partial reduction of Suv420h1 (fig. S1, A and B) or to compensation by Myf5-independent muscle cells (*40*–*42*).

We used high-resolution respirometry to evaluate the metabolic activity of equal amounts of mitochondria isolated from dKO and control iBAT (Fig. 1B). While there was no significant difference in oxygen consumption after the addition of glutamate-malate (state 2), compared to controls, dKO mice displayed a significant increase in

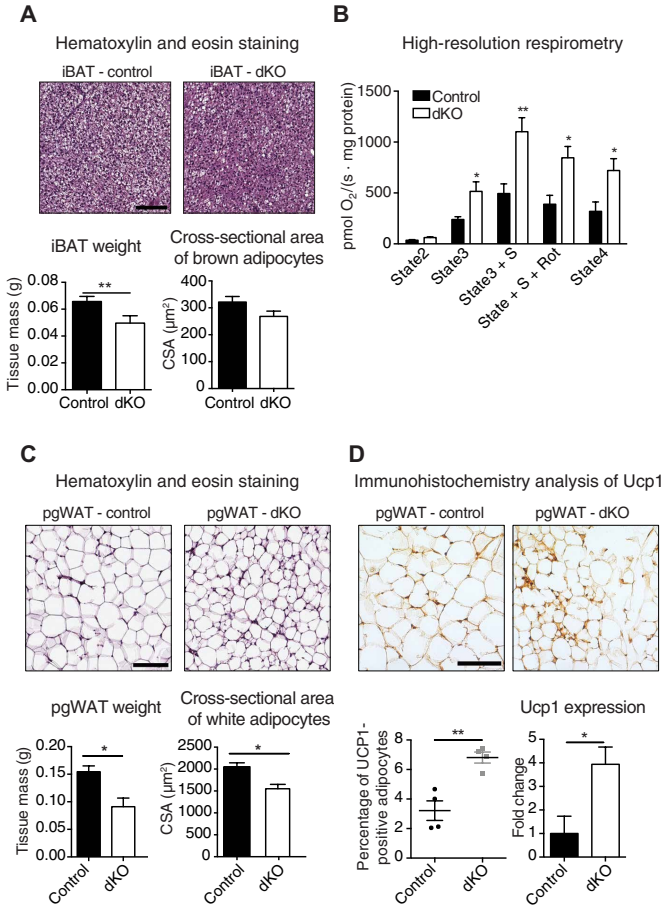

Fig. 1. Characterization of Suv420h dKO mice. (**A**) Top: H&E stains (20×) of paraffin-embedded sections representative of iBAT. Scale bar, 100 mm. Bottom: Quantification of the mass of iBAT and cross-sectional area (CSA) of brown adipocytes ($n = 3$, males, 4 weeks old). (**B**) Mitochondria respiratory rates of isolated mitochondria. BAT from controls and dKO mice was dissected and brown adipocytes were isolated. Then, mitochondria were extracted and used into the O2K oxygraph chambers [mean ± SEM; one-way analysis of variance (ANOVA); $^*P < 0.05$] ($n = 6$ per genotype). (**C**) Top: H&E stains (20×) of pgWAT ($n = 3$, males, 4 weeks old). Scale bar, 100 mm. Bottom: Quantification of the mass of pgWAT (left) and quantification of the cross-sectional area of white adipocytes (right) ($n = 3$, males, 4 weeks old). (**D**) Top: Immunohistochemistry for Ucp1 on pgWAT of control and dKO mice. Scale bar, 100 mm. Bottom: Quantification of the percentage of Ucp1-stained area (left) and RT-qPCR analysis of Ucp1 expression levels in control and dKO mice (right) ($n = 3$, males, 4 weeks old). Values are expressed as mean ± SEM; *t* test; $^*P < 0.05$; $^{**}P < 0.01$.

maximal mitochondrial oxygen consumption after the addition of saturating concentrations of adenosine diphosphate (ADP) (state 3), and this increase persisted after the consecutive addition of succinate alone (state 3 + Succ) or succinate and rotenone (state 3 + Succ + Rot) and in resting respiration (state 4) (Fig. 1B). These data indicate that the entire respiratory chain is significantly increased in iBAT mitochondria adipocytes of dKO mice compared to controls, in line with an enhanced metabolic activity of dKO brown adipocytes.

Suv420h dKO mice have reduced white fat mass and increased browning

Histological analyses of WAT revealed significantly smaller adipocytes and a significant reduction of weight in perigonadal WAT (pgWAT) from dKO compared to control mice (Fig. 1C). Noticeably, pgWAT adipocytes of dKO mice showed clustered populations of cells with smaller multilocular lipid droplets (Fig. 1C), a characteristic of WAT browning (*8*). Immunohistochemistry and reverse transcriptase quantitative polymerase chain reaction (RT-qPCR) demonstrated significantly higher areas of Ucp1-positive adipocytes and a significant increase in Ucp1 expression in pgWAT from dKO compared to control mice (Fig. 1D), supporting increased browning of pgWAT in dKO mice.

Suv420h dKO mice have increased metabolic parameters

Given that activated brown/beige fat affects whole-body glucose homeostasis, we measured blood glucose levels. We found that dKO mice have significantly lower basal glycemia compared to controls (Fig. 2A). In glucose tolerance tests (GTTs), when challenged with intraperitoneal glucose injection, dKO mice tolerate the glucose overload significantly better than control mice (Fig. 2B).

To assess whether lack of Suv420h also resulted in an altered thermogenic response, we conducted acute cold challenge experiments. We found that the expression of Suv420h1 and Suv420h2 in iBAT is significantly reduced by cold exposure (Fig. 2C). This is associated to a significant decrease of H4K20me3 in iBAT of cold-exposed animals compared to controls (fig. S2). Notably, compared to controls, dKO mice exposed to cold display a significantly higher increase in iBAT expression of key genes for non-shivering thermogenesis such as Ucp1, Pgc1a, and Dio2 (Fig. 2D) (*43*) and have no difficulty in maintaining their body temperature (Fig. 2, E and F). Collectively, our results indicate that Suv420h1 and Suv420h2 respond to temperature exposure and control BAT thermogenic and glucose-modulatory activities.

Suv420h depletion results in BAT transcriptional changes consistent with increased metabolic activity

To gain insight into the pathways affected by Suv420h deletion, we compared dKO to control iBAT using RNA sequencing (RNA-seq). Among the 10,731 genes detected by the RNA-seq as being "expressed," a total of 1049 (9.7%) were significantly altered in dKO compared to control mice (table S1 under the sheet "RNA-seq Young"). In line with the repressor activity of Suv420h proteins, Suv420h ablation resulted in a significant majority of up-regulated genes (618 up-regulated, 431 down-regulated, binomial $P = 9 \times 10^{-9}$) (Fig. 3A). Functional enrichment analysis for the up-regulated genes returned significant enrichment for oxidative metabolism and mitochondrial function pathways (Fig. 3B and table S2). We also found significant enrichment of genes related to proteasomal activity, which was recently shown to be required for BAT thermogenic function (Fig. 3B) (*44*). Up-regulation of representative genes in iBAT of dKO mice compared to controls (Fig. 3C) was confirmed by RT-qPCR (fig. S3A). Functional enrichment analysis for the down-regulated genes failed to return relevant pathways (fig. S3B).

Suv420h dKO mice are less susceptible to obesity

Our results support increased metabolic activity in Suv420h dKO mice. We thus evaluated how dKO mice respond to obesity induced by high-fat diet (HFD). Over 14 weeks of eating an HFD, control mice gained 48.5% more weight when eating HFD versus normal diet compared to dKO mice (Fig. 4A), despite dKO mice consuming significantly more energy compared to controls (Fig. 4B). At the end of the HFD treatment, controls were significantly heavier compared to dKO mice (Fig. 4C). This indicates that dKO mice eating an HFD are less metabolically efficient than control mice, which is indeed the case (Fig. 4D). Live-animal magnetic resonance imaging (MRI) quantification revealed smaller posterior subcutaneous WAT (psWAT) and pgWAT depots in HFD dKO compared to control mice (Fig. 4E). Histological analyses showed significantly reduced adipocyte size in both iBAT and pgWAT of dKO mice compared to controls (Fig. 4, F and G). Together, these results demonstrate that dKO mice are less affected by diet-induced obesity (DIO).

To identify gene expression changes that might account for dKO protection from DIO, we compared the transcriptomes of Suv420h-deficient to control iBAT in the different diet regimens. RNA-seq revealed 1011 genes significantly altered in the dKO compared to the control genotype regardless of the diet (table S1 under the sheet "RNA-seq Diet"), of which the significant majority was up-regulated (558 up-regulated, 453 down-regulated, binomal $P = 0.001$) (Fig. 5A). Functional enrichment analysis of the up-regulated genes uncovered significant enrichment for metabolism, fatty acid oxidation, branched chain amino acid (BCAA) catabolism, and secretion of protein pathways (Fig. 5B and table S2). The expression of genes encoding for BCAA catabolic enzymes is significantly decreased in the adipose tissue of patients with obesity and diabetes (*45*). The subsequent increased plasma level of BCAA and toxic intermediates has been suggested to cause insulin resistance (*45*). Up-regulation of representative genes for the identified pathways in iBAT of dKO compared to control mice (Fig. 5C) was confirmed by RT-qPCR at the end of both feeding regimens (fig. S4). Functional enrichment analysis for the down-regulated genes returned cholesterol biosynthesis as a relevant pathway, which is in line with the phenotype of dKO mice (fig. S5).

Correlation analysis reported a significant overlap between the gene expression changes detected in RNA-seq Young and RNA-seq Diet (fig. S6, A to C). Together, our observations suggest that Suv420h proteins are involved in repression of genes, which, when up-regulated, confer protection from obesity.

PPAR-γ is a direct Suv420h target

Genes up-regulated in Suv420h dKO BAT show significant enrichment for PPAR signaling pathway (table S2). In addition, chromatin immunoprecipitation sequencing (ChIP-Seq) enrichment analysis (ChEA) indicates a significant enrichment in PPAR-γ target genes for up-regulated genes in Suv420h dKO BAT (table S3). We further tested the functional correlation of the genes up-regulated in dKO mice with PPAR-γ target genes by using GSEA (Gene Set Enrichment Analysis). Figure 6A shows that PPAR-γ targets are significantly correlated to genes up-regulated in dKO mice in both

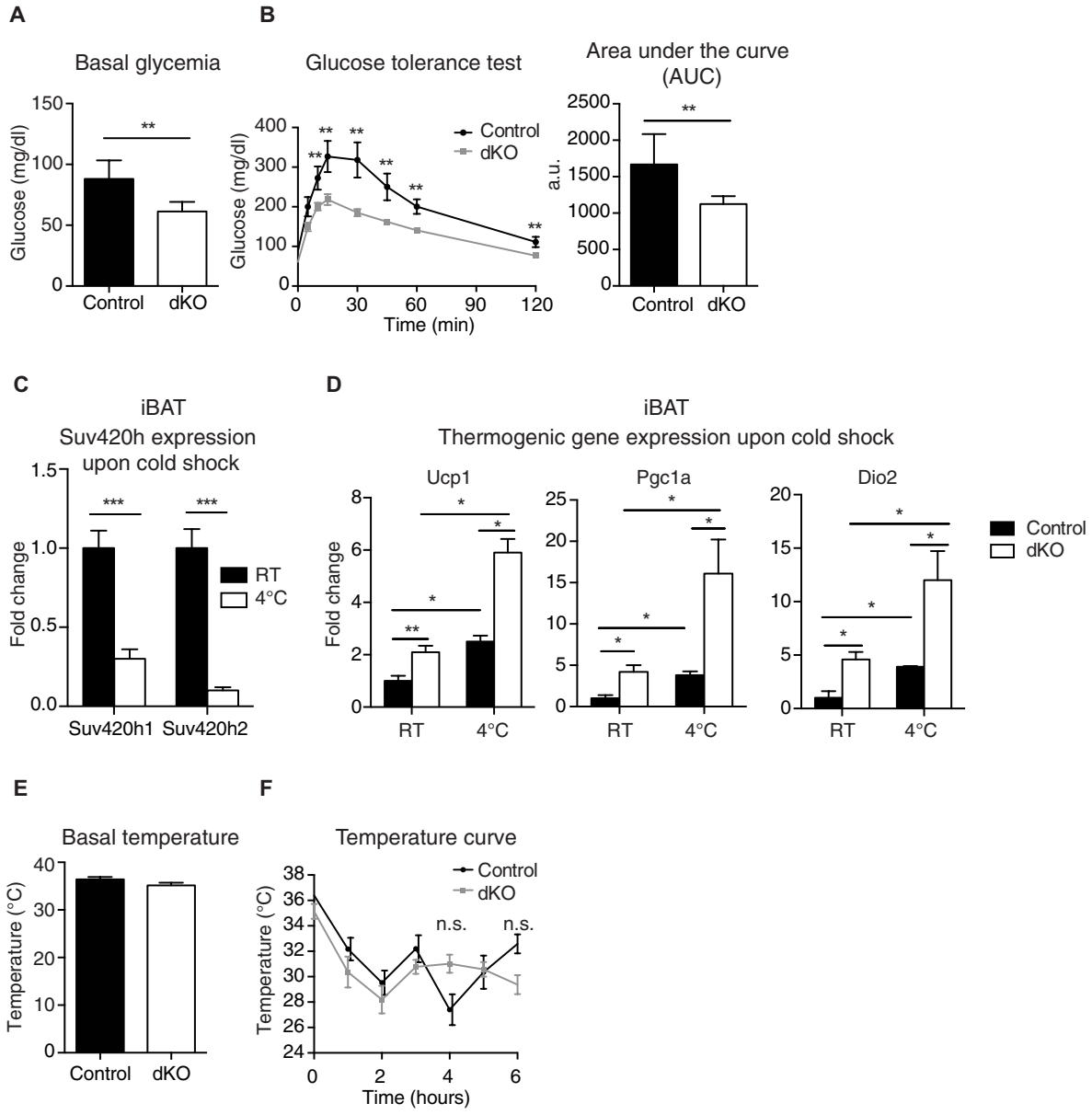

Fig. 2. Suv420h dKO mice have improved metabolic parameters. (**A**) Basal glycemia measured in overnight-fasted control and dKO mice ($n = 6$ per genotype). Glucose levels were measured from the tail vein using a standard glucometer. (**B**) GTT performed in control and dKO mice after overnight fasting. The test was performed by intraperitoneally injecting D-glucose (2 g/kg). Blood glucose levels were measured at the indicated time points (5, 10, 15, 30, 45, 60, and 120 min after glucose administration) from the tail vein using a standard glucometer ($n = 6$ per genotype). a.u., arbitrary units. (**C** and **D**) Gene expression analysis of Suv420h1, Suv420h2, Ucp1, Pgc1a, and Dio2 mRNA by RT-qPCR performed in iBAT of mice with or without cold exposure ($n = 6$ per genotype). (**E** and **F**) Left: Basal core rectal temperature of control and dKO mice recorded at room temperature (RT) using a rectal probe (RET-3, ThermoWorks). Right: Rectal temperature in acute cold challenge (right) ($n = 6$ per genotype) measured hourly for 6 hours. Values are expressed as mean ± SEM; *t* test;*$P < 0.05$; **$P < 0.01$; ***$P < 0.001$. n.s., not significant.

RNA-seq Young (ND) and RNA-seq Diet (HFD). Moreover, we calculated the overlap of up-regulated genes in Suv420h dKO in both RNA-seq Young and RNA-seq Diet, with a comprehensive dataset of PPAR-γ targets generated considering (i) genes identified in PPAR-γ ChIP experiments, (ii) genes up-regulated after PPAR-γ overexpression, (iii) genes up-regulated upon PPAR-γ agonist stimulation, (iv) PPAR-γ signaling pathway genes, and (v) genes coexpressed with PPAR-γ (table S3). Using this comprehensive list of PPAR-γ targets generated using different empirical sources for the RNA-seq Young, we found that 61% of up-regulated genes in Suv420h dKO overlap with PPAR-γ targets representing an odds ratio of enrichment of 2.1 [95% confidence interval (CI), 1.75 to 2.45; Fisher $P < 2.2 \times 10^{-16}$]. For the RNA-seq Diet, we again found a highly significant overlap with 52% of up-regulated genes in Suv420h dKO overlapping with PPAR-γ targets (odds ratio, 1.6; 95% CI, 1.37 to 1.93; Fisher $P = 3.1 \times 10^{-8}$). These results strongly support the enrichment for PPAR-γ targets in genes up-regulated in Suv420h dKO iBAT.

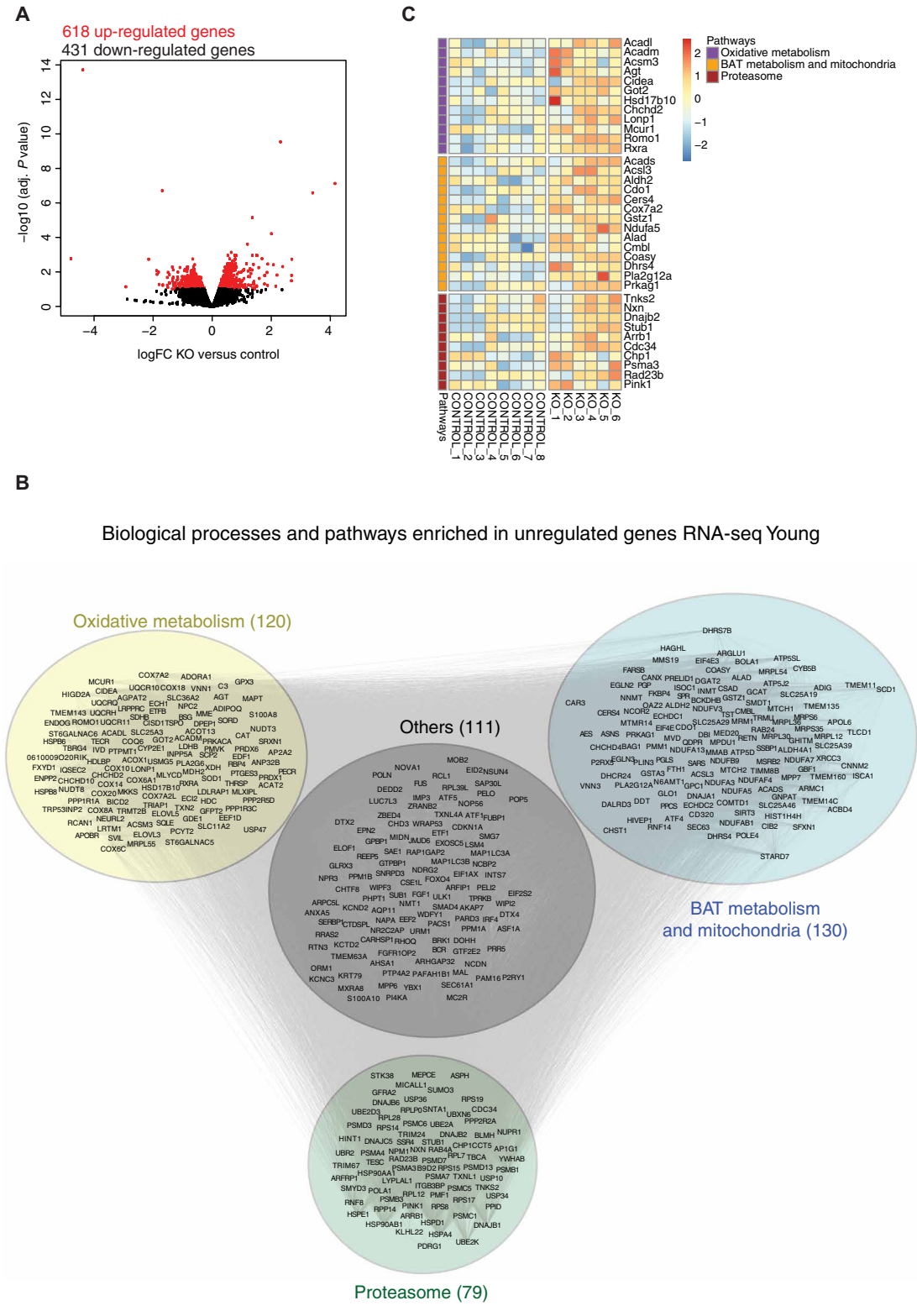

Fig. 3. Transcriptional changes in dKO mice. (**A**) Volcano plot showing the significance of differentially expressed genes in iBAT of dKO versus control mice in RNA-seq Young. The total number of up-regulated (red) and down-regulated (black) genes is shown above the plot. Red dots are considered significant with an adjusted $P < 0.1$. (**B**) Network representation of functional enriched biological processes and pathways. Up-regulated genes in dKO were found enriched in several pathways [Enrichr, Fisher Test; false discovery rate (FDR) < 0.05, table S2] and grouped on the basis of the pathways they belong to. Pathways and processes were further grouped into four higher hierarchy super pathways after visually inspecting the clusters. The number of genes contained in each super pathway is shown in parentheses next to the pathway name. (**C**) Heatmap of normalized (*Z* score on samples) levels of expression of RT-qPCR–validated genes (in fig. S3) grouped by the three super clusters of interest in (B).

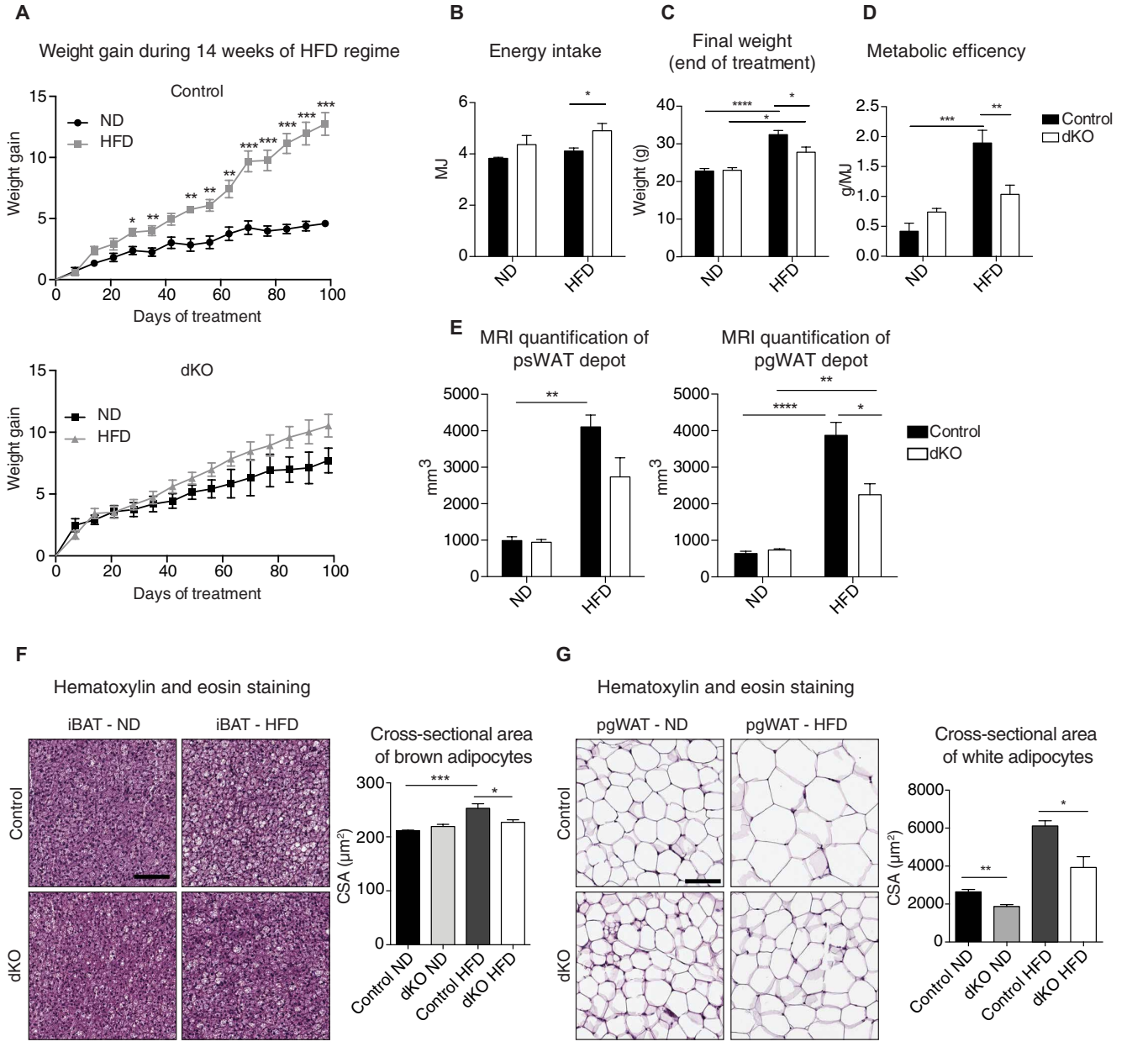

Fig. 4. Suv420h dKO mice are resistant to diet-induced obesity. (**A**) Weight gain of control and dKO mice during 14 weeks of normal diet (ND) or HFD ($n = 6$ for both genotypes in both diets). Body weight was measured weekly for 14 weeks of treatment. Weight gain is represented as percentage of initial weight. (**B**) Total energy intake (MJ) during the feeding regimen in (A) ($n = 6$ for both genotypes in both diets). Food intake was measured weekly during both feeding regimens. At the end of the experiment, total energy intake was calculated on the basis of the energy content of the two diets. (**C**) Final weight of the mice at the end of the feeding regimen in (A) ($n = 6$ for both genotypes in both diets). Bar graph represents the weight of the mice at the end of the experiment. (**D**) Metabolic efficiency determined as the amount of body weight increase (g) per megajoule of food consumed in both diets ($n = 6$ for both genotypes in both diets). (**E**) MRI analysis of subcutaneous and perigonadal (psWAT and pgWAT, respectively) WAT of control and dKO mice 1 week before the end of the feeding regimen in (A) ($n = 6$ for both genotypes in both diets). (**F** and **G**) H&E staining of iBAT (F) and pgWAT (G) of control and dKO mice after 14 weeks of eating chow (ND) or HFD. Scale bar, 100 mm. The bar graphs show that dKO mice adipocytes are smaller than those of control mice even upon HFD feeding ($n = 6$ for both genotypes in both diets). Values are expressed as mean ± SEM; *t* test; $^*P < 0.05$, $^{**}P < 0.01$, $^{***}P < 0.001$, $^{****}P < 0.0001$.

Supporting the above findings, we found that PPAR-γ is significantly up-regulated compared to controls in all conditions showing decreased Suv420h (Fig. 6, C to L). PPAR-γ is augmented significantly in iBAT of young dKO compared to control mice (Fig. 6C) and in both diet regimens (Fig. 6D). Moreover, PPAR-γ levels significantly increase upon cold exposure (Fig. 6E), concomitant with Suv420h down-regulation (Fig. 2C). ChIP followed by quantitative real-time PCR (ChIP-qPCR), showed that the Suv420h-associated histone mark H4K20me3 decreases at the PPAR-γ gene in iBAT upon cold exposure (Fig. 6F). ChIP-qPCR also showed that H4K20me3 is enriched at the PPAR-γ gene in proliferating brown pre-adipocytes (Fig. 6G), in which PPAR-γ is normally repressed

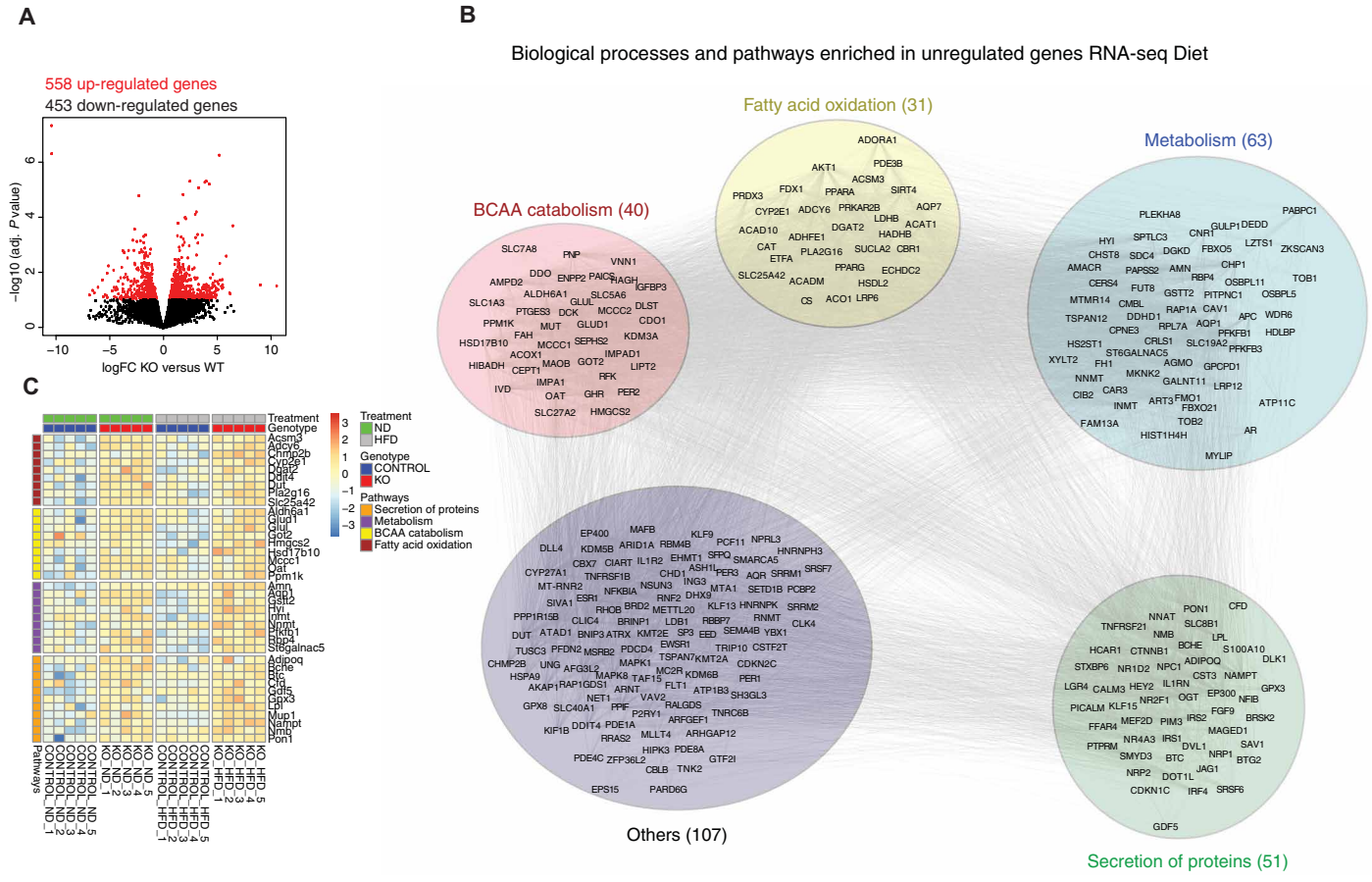

Fig. 5. Transcriptional changes in dKO mice after HFD regimen. (**A**) Volcano plot showing the significance of differentially expressed genes in iBAT of dKO versus WT in RNA-seq Diet. The total number of up-regulated (red) and down-regulated (black) genes is shown above the plot. Red dots are considered significant with an adjusted $P < 0.1$. (**B**) Network representation of functional enriched biological processes and pathways. Up-regulated genes in dKO were found enriched in several pathways (Enrichr, Fisher Test; FDR < 0.05, table S2) and grouped on the basis of the pathways they belong to. Pathways and processes were further grouped into five higher hierarchy super pathways after visually inspecting the clusters. The number of genes contained in each super pathway is shown in parentheses next to the pathway name. (**C**) Heatmap of normalized (*Z* score on samples) levels of expression of RT-qPCR–validated genes (in fig. S5) grouped by the three super clusters of interest in (B).

(*46*). Treatment with the Suv420h-specific inhibitor A-196 (*47*) significantly abrogates H4K20me3 at the PPAR-γ gene (Fig. 6G) and leads to a significant increase in PPAR-γ expression level compared to vehicle-treated cells [dimethyl sulfoxide (DMSO)] (Fig. 6H). These results suggest that PPAR-γ is a direct Suv420h target, which could play an important role in Suv420h metabolic regulation. Accordingly, treatment of proliferating brown pre-adipocytes with A-196 is sufficient to significantly activate the expression of PPAR-γ direct target genes (Fig. 6I), which is blocked by concomitant treatment with a specific PPAR-γ inhibitor. Moreover, A-196 treatment leads to a significant increase of the respiratory rate of brown pre-adipocytes (Fig. 6L), and this effect depends on PPAR-γ since it is blocked by treatment with the PPAR-γ inhibitor (Fig. 6L). In summary, our results indicate that Suv420h proteins respond to environmental stimuli by regulating PPAR-γ expression and pathways important for energy expenditure and obesity.

DISCUSSION

There is increasing interest in understanding the mechanisms regulating BAT function, with the goal of controlling energy expenditure to fight obesity and comorbidities. Since the discovery of appreciable amounts of BAT in human adults (*6*), major attention has been focused toward developing ways to manipulate BAT activity for the treatment of metabolic syndrome. Elucidation of these regulatory mechanisms may provide novel targets for therapeutics. Epigenetics has emerged as an exciting area for drug development because epigenetic enzymes have the capacity to integrate gene expression with the metabolic state of the cell and are often aberrantly expressed in human disease (*48*, *49*).

Here, we have demonstrated that Suv420h ablation activates BAT metabolism, resulting in improved metabolic parameters and systemic protection against obesity. Previous studies also provided indirect evidence supporting a possible role for Suv420h enzymes in metabolism regulation and in intergenerational transmission of metabolic programming (*22*). Nevertheless, a direct evaluation of the role of Suv420h in adipose tissue was not available thus far. To our knowledge, our study provides the first demonstration of a direct role for Suv420h enzymes in the regulation of metabolism. While there are likely other direct Suv420h targets that could contribute to the phenotype of dKO mice, our data strongly suggest that PPAR-γ is a key mediator of Suv420h metabolic activity.

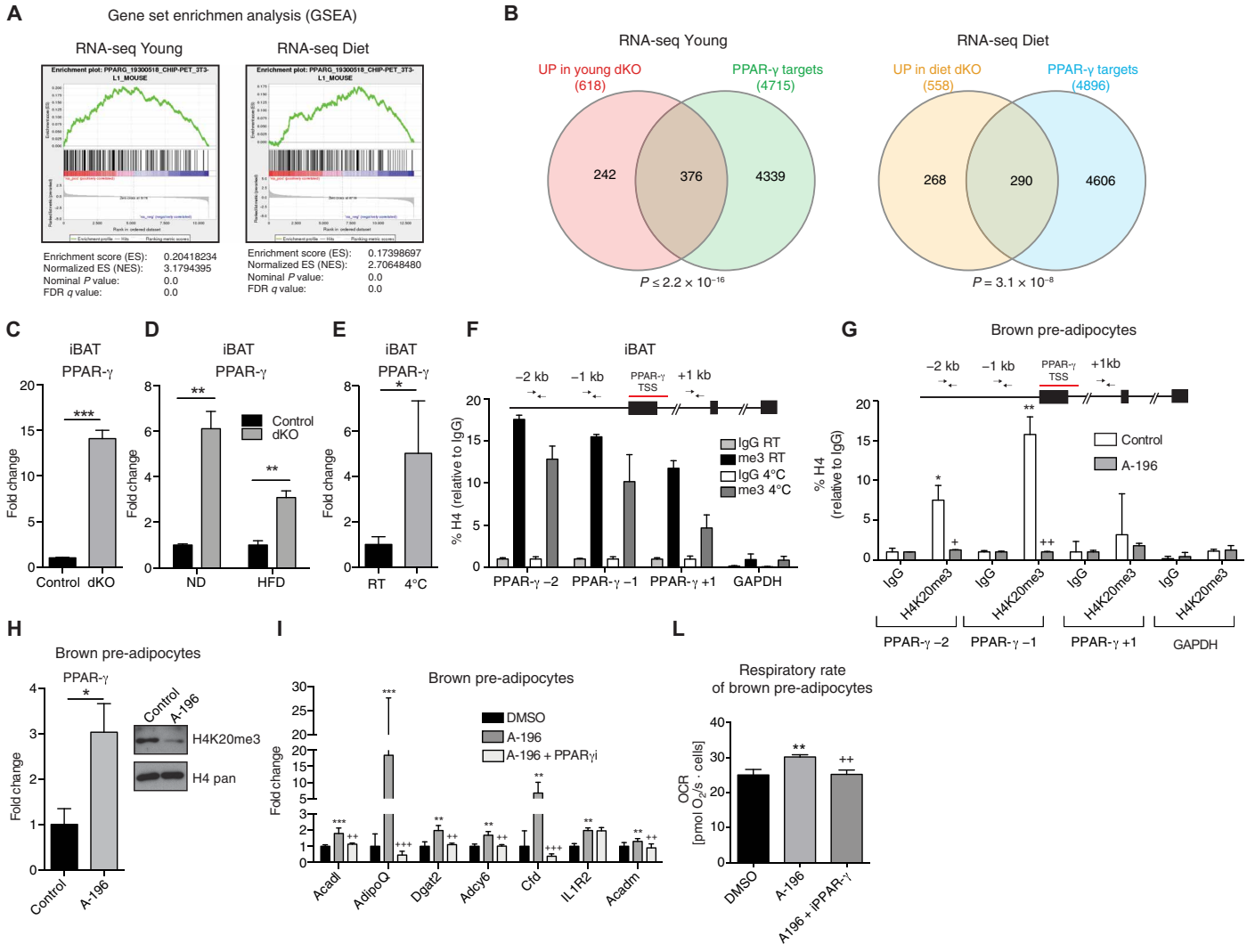

Fig. 6. PPAR-γ is a direct target of Suv420h. (**A**) GSEA of PPAR-γ targets in the ChIP-PET (pair end-tagging) experiment in mouse from the ChEA database for RNA-seq Young (left) and RNA-seq Diet (right). (**B**) Venn diagram showing the overlap of genes up-regulated in Suv420h dKO with a comprehensive dataset of PPAR-γ targets as defined in Materials and Methods. (**C** to **E**) RT-qPCR for PPAR-γ expression in the indicated experimental condition [$n = 3$ controls and $n = 7$ dKO in (C); $n = 6$ for both genotypes and feeding conditions in (D); $n = 6$ for both conditions in (E)]. (C) RT-qPCR for PPAR-γ expression in iBAT from control and dKO mice. (D) RT-qPCR for PPAR-γ expression in iBAT from mice used in the DIO (see Fig. 4) experiment, after 14 weeks of HFD regimen. Control mice were fed with standard chow (ND, normal diet). (E) RT-qPCR for PPAR-γ expression in iBAT from mice with or without cold exposure (see Fig. 2, E and F). (**F** and **G**) ChIP assays using the indicated antibodies analyzed by qPCR using primers located on the PPAR-γ and glyceraldehyde phosphate dehydrogenase (GAPDH) (used as negative control) genomic regions as shown by the scheme above each graph ($n = 3$). (F) ChIP-qPCR performed in iBAT dissected from mice with or without cold exposure. The day before the experiment, mice were grouped in cages with water and bedding, and starved overnight. On the day of the experiment, mice were placed either at room temperature or at 4°C for 6 hours. At the end of the treatment, mice were euthanized, and iBAT was isolated. Chromatin was extracted from iBAT as described in Materials and Methods and used for ChIP. (G) ChIP-qPCR performed in proliferating brown pre-adipocytes treated for 7 days with either the Suv420h inhibitor A-196 (10 mM) or DMSO, as control. IgG, immunoglobulin G. (**H**) RT-qPCR for PPAR-γ expression in brown pre-adipocytes treated for 7 days with the Suv420h-specific inhibitor A-196 (10 mM) ($n = 4$) (left). Representative Western blot showing decrease of H4K20me3 upon treatment (right). (**I**) RT-qPCR expression analysis of the indicated PPAR-γ target genes in brown pre-adipocytes treated with A-196 (10 mM) alone or in combination with the iPPAR-γ (10 μM) ($n = 3$). For A to I, values are expressed as mean ± SEM; *t* test. (**L**) Oxygen Consumption Rate (OCR) measurement in proliferating brown pre-adipocytes treated with A-196 (10 μM) alone or in combination with the iPPAR-γ (10 mM) (mean ± SEM; one-way ANOVA) ($n = 5$). $^{*}P < 0.05$, $^{**}P < 0.01$, $^{***}P < 0.001$, $^{++}P < 0.01$ relative to A-196; $^{+++}P < 0.001$ relative to A-196.

PPAR-γ is a nuclear receptor that regulates lipid metabolism, glucose homeostasis, and energy balance (*50*). Synthetic PPAR-γ ligands of the TZD class are used as insulin sensitizers in the treatment of diabetes (*51*, *52*). Yet, their use has been limited by adverse effects, such as heart failure, weight gain, fluid retention, and bone fragility (*53*). Notably, there are several mechanisms contributing to weight gain associated to systemic PPAR-γ activation. Weight gain may result from increased body fat. This is adipose depot specific, since TZDs have been shown to induce reduction of visceral fat but to increase subcutaneous fat. An additional mechanism influencing body weight gain upon systemic PPAR-γ activation is increased body fluid volume due to water retention. In addition, this process

is tissue and cell type specific, given that PPAR-γ deletion selectively in kidney or in endothelial cells blocks TZD-induced weight gain in animal models (*54*–*56*). TZD-mediated activation of PPAR-γ also leads to increased feeding due to a tissue-specific activity mediated by PPAR-γ in the central nervous system (*57*). Hence, it is tempting to speculate that we did not observe weight gain in Suv420h dKO mice due to the tissue-restricted PPAR-γ activation supporting the notion that targeting Suv420h could help dissociate the benefit of PPAR-γ activation from its side effect. Suv420h dKO mice display transcriptomic changes with a strong PPAR-γ signature, resulting in the up-regulation of several PPAR-γ target genes relevant for BAT metabolic functions. Pharmacological Suv420h inhibition is not toxic to brown adipocytes and is sufficient to activate PPAR-γ expression and mitochondria respiration. However, systemic inhibition of Suv420h activity in vivo might be unfeasible due to the embryonic lethality of Suv420h1 KO mice (*20*). Future work devoted to developing ways to target Suv420h specifically in BAT could help overcome this issue. Alternatively, direct Suv420h epigenetic targets important for bioenergetics and metabolism selectively expressed in BAT could be targeted to achieve safe and effective therapeutics. In this respect, it is important to notice that Suv420h depletion is associated with several systemic effects including WAT browning. Among the genes significantly up-regulated in Suv420h dKO mice, we found several genes encoding for secreted proteins with endocrine function known to act on other tissues to stimulate energy expenditure, such as lpl (*58*), mup1 (*59*), and gdf5 (*60*). Based on this, it is tempting to speculate that increased production of a number of BAT-derived secreted molecules could have a systemic effect on other tissues contributing to the consequences of Suv420h ablation.

We found that the expression of both Suv420h1 and Suv420h2 is significantly down-regulated in BAT by cold exposure, which has been confirmed by a very recent publication (*61*). Suv420h2 and H4K20me3 have been found to be up-regulated by hyperglycemia (*24*). Together, these results suggest that Suv420h expression and/or activity could constitute a nexus between environmental stimuli and the epigenetic regulation of metabolism.

Our results indicate that only by deleting both Suv420h1 and Suv420h2 can we completely abrogate H4K20me3 in BAT. Nevertheless, we cannot exclude the idea that single KO for either Suv420h1 or Suv420h2 genes might be sufficient to observe alterations of metabolic features. Future work might evaluate the individual contribution of Suv420h1 and Suv420h2 to metabolism regulation and obesity susceptibility. In summary, our results support a key role for Suv420h enzymes in the epigenetic regulation of the pathways controlling metabolism in response to environmental stimuli and as new potential targets for metabolic disorders.

MATERIALS AND METHODS

Generation of Suv420h dKO mice

All animal procedures were approved by the Institutional Animal Care and Use Committee of IRCCS (Istituto di Ricerca e Cura a Carattere Scientifico) San Raffaele Scientific Institute and were communicated to the Italian Ministry of Health and local authorities according to Italian law. Mice were housed and maintained on a 12-hour light/12-hour dark cycle at constant temperature (23°C). Food and water were available ad libitum. To obtain Suv420h1$^{-/-}$_Suv420h2$^{-/-}$ dKO mice, Suv420h1$^{flox/flox}$ and Suv420h2$^{-/-}$ mice (*20*) were bred with Myf5-Cre mice (JAX stock 007893), in which the cre recombinase gene was driven by the Myf5 promoter. All animals were of the C57Bl/6J genetic background. Unless differently stated, age-matched female mice between 4 and 8 months were used for experiments.

Metabolic studies

For DIO studies, 7-week-old mice were fed either regular chow (ND) or an HFD (E15744-34, 45 kJ% fat, Charles River) for 14 weeks. Body weight and food intake were measured weekly. For the glucose tolerance test experiment, mice fasted for 16 hours were injected intraperitoneally with D-glucose (2 g/kg). Blood glucose levels were measured from the tail vein at the indicated times using a standard glucometer.

Adipose tissue measurement by magnetic resonance

MRI was performed with a dedicated horizontal 7-T scanner (Bruker, BioSpec 70/30 USR, Paravision 5.1; Germany). High-resolution T1-weighted sequences with and without fat saturation were acquired covering a body region from the hepatic dome to the inguinal canal. By means of image subtraction (T1 – T1 fat), a "pure fat" result stack was obtained, on which a mask definition of adipose tissue along the abdominal fascia was manually drawn to separately segment the intraperitoneal/retroperitoneal perigonadal fat compartment and the subcutaneous one. After abdominal adipose tissue segmentation, volume quantification was semi-automatically performed using a region growing function. Image processing and all the analyses were performed by a radiologist with experience in preclinical imaging, using MIPAV Open Source Software v.5.3.4 (https://mipav.cit.nih.gov/index.php).

Cold exposure experiment

For cold exposure experiments, mice fasted overnight (16 hours) were kept in a cold room (4°C). The core body temperature was recorded hourly for 6 hours using a rectal probe (RET-3, ThermoWorks). At the end of the experiment, mice were euthanized for subsequent biochemical experiments.

Histology analysis

For H&E staining, iBAT and pgWAT were fixed in 10% neutral-buffered formalin. Samples were then embedded and processed for staining by the San Raffaele Mouse Clinic according to standard procedures. Section images were acquired with an Aperio Digital Pathology Slide Scanner, and the cross-sectional area (CSA) of adipocytes was evaluated using ImageScope software.

For immunohistochemistry, pgWAT sections were rehydrated at room temperature, and antigen retrieval was performed using 10 mM Na-citrate (pH 6; S1804, Sigma-Aldrich). Endogenous peroxidase was inhibited by incubation for 10 min at room temperature with methanol and 0.03% hydrogen peroxide. Then, sections were incubated overnight at 4°C with anti-Ucp1 antibody (1:500 dilution; ab10983, Abcam). Then, samples were incubated with 1:500 dilution of a secondary antibody conjugated with biotin (E0432, Dako). An avidin-biotin-peroxidase complex was added (Vector Lab, Burlingame, CA), and sections were incubated for 5 to 10 min with a DAB (3,3′-diaminobenzidine) substrate (Dako, Glostrup, Denmark).

Gomori trichrome staining on skeletal muscle was performed as previously described (*62*). CSA analysis was performed using ImageJ software.

Cell culture and treatment

Immortalized brown pre-adipocytes (*47*) were cultured in DMEM/F12 supplemented with 10% fetal bovine serum. For inhibitor treatment, cells were plated at 50% confluence. The A-196 inhibitor was dissolved in DMSO and added to the culture medium (final concentration of 10 μM) for 7 days. For double treatment, iPPAR-γ (Selleckchem T0070907) was added to A-196–treated cells at day 5 at a final concentration of 10 μM. Control cells were treated with DMSO alone. At day 7, cells were collected and used for Western blot, RNA extraction, and RT-qPCR analysis (see below). For respirometry assays, cells were collected and processed as described below.

Western blot

For analysis of the Suv420h histone mark in fig. S1C, BAT was dissected from wild-type C57/Bl6, Myf5-Cre, Suv420h1 single-KO (sKO1), Suv420h2 single-KO (sKO2), and dKO mice (fig. S1C, three per genotype). To analyze the Suv420h histone mark after cold challenge (fig. S2), wild-type C57/Bl6 mice were placed at either room temperature or 4°C for 6 hours before they were euthanized. For both experiments, BAT was lysed using a dounce homogenizer in Triton extraction buffer [TEB: PBS (phosphate-buffered saline) containing 0.5% Triton X-100 (v/v)] and kept for 10 min on ice. Samples were centrifuged at 6500*g* for 10 min at 4°C. The pellets were then washed in half of TEB and centrifuged as before. Acid extraction was carried out overnight at 4°C by resuspending the pellet in 0.2 N HCl. The day after, samples were centrifuged at 6500*g* and the supernatant was collected and neutralized with 2 M NaOH at $^1/_{10}$ of the volume of the supernatant.

Samples were separated on 15% acrylamide gel, and the membrane was decorated using anti-H4 and anti-H4K20me3 antibodies (table S4). IRDye 800CW secondary antibody was used in combination with Odyssey Imaging Systems. Quantification of the ratio H4K20me3 over H4 total was performed using Odyssey Imaging Systems software.

Oxygen consumption measurement

Mitochondria respiratory rates were measured into the O_2K oxygraph chambers (Oroboros, Instruments Oroboros, Innsbruck, Austria) at 37°C in the respiration medium MiR06 [0.5 mM EGTA, 3 mM $MgCl_2$, 60 mM K-lactobionate, 20 mM taurine, 10 mM KH_2PO_4, 20 mM Hepes, 110 mM sucrose, fatty acid–free bovine serum albumin (1 g/liter), and catalase (280 U/ml) (pH 7.1)]. To detect the electron flow through respiratory chain complexes, titrations of all of substrates, uncouplers, and inhibitors were added in series as previously reported (*63*, *64*).

Briefly, we added pyruvate (10 mM) and malate (2 mM) to obtain state 2 respiration. Then, we injected ADP (2.5 mM) to evaluate state 3 respiration, and the further addition of succinate (10 mM) allowed the measurement of complex I (CI)– and CII-driven respiration (state3 + Succ). Then, CI was inhibited by injecting rotenone (0.5 μM) (state3 + Succ+ Rot) and state 4 was measured by administration of oligomycin (2 μg/ml). Last, we added antimycin A (2.5 μM) to inhibit CIII obtaining a residual oxygen consumption. Cytochrome c (10 μM) was added to test the integrity of the outer mitochondrial membrane. Oxygen fluxes were corrected by subtracting residual oxygen consumption from each steady state.

For experiments with cell culture, 1×10^6 viable cells were transferred into oxygraph chambers. When oxygen consumption reached a plateau, a steady-state level was obtained displaying routine respiration. The addition of oligomycin (0.5 μM) resulted in leak respiration. Subsequently, the proton gradient was released by stepwise titration (0.5 μM each step) of the uncoupler carbonyl cyanide-4-(trifluoromethoxyphenylhydrazone) until the maximum respiration was achieved. The addition of 0.5 μM rotenone and 2.5 μM antimycin A blocked mitochondrial respiration, showing residual oxygen consumption. Initial addition of pyruvate (10 mM) and malate (2 mM) was performed to test the integrity of the plasma membrane. Oxygen fluxes were corrected by subtracting residual oxygen consumption from each steady state.

RNA extraction and RT-qPCR analysis

Total RNA was extracted and treated with deoxyribonuclease I, using TRIzol reagent (Thermo Fisher Scientific). cDNA was synthesized using Invitrogen's SuperScript III First-Strand Synthesis SuperMix. qPCRs were performed with SYBR GreenER qPCR SuperMix Universal (Invitrogen) using the CFX384 Real-Time PCR Detection System (Bio-Rad). Relative quantification was calculated with CFX Manager Software V.1.6. TATA-binding protein (Tbp) was used as housekeeping gene for sample normalization. The Student's *t* test was used to evaluate statistical significance. Primers were designed using Primer3 tool (http://primer3.ut.ee) and are listed in table S4.

Chromatin immunoprecipitation

For chromatin isolation from BAT, dissected tissues were pulled together, minced, and homogenized using a dounce. Cross-linking was performed by adding formaldehyde (Sigma-Aldrich) to a final concentration of 1% in PBS for 10 min at room temperature. After formaldehyde quenching with 125 mM glycine (Sigma-Aldrich) for 5 min, isolated cells were centrifuged at 1350*g* for 10 min at 4°C. Pellet was lysed in Wash Buffer (WB) 1 solution [10 mM tris-HCl (pH 8), 0.25% Triton, 1 mM EDTA, and 0.5 mM EGTA] for 10 min on ice. The samples were centrifuged at 1350*g* for 5 min at 4°C. The resulting pellet was washed in 1 ml of WB2 solution [10 mM tris-HCl (pH 8), 200 mM NaCl, 1 mM EDTA, and 0.5 mM EGTA] for 10 min at 4°C. Next, samples were centrifuged at 1350*g* for 5 min at 4°C, and the resulting pellet was lysed in WB3 solution [15 mM tris-HCl (pH 8), 10 mM EDTA, and 1% SDS]. WB1, WB2, and WB3 solutions were supplemented with protease inhibitor (Complete EDTA-free Protease Inhibitor Cocktail Tablets, Roche).

Brown pre-adipocytes were cross-linked by directly adding formaldehyde to the medium (Sigma-Aldrich) to a final concentration of 1%. Cells were incubated with gentle swirl 10 min at room temperature. After formaldehyde quenching with 125 mM glycine (Sigma-Aldrich) for 5 min, cells were washed with PBS and harvested by scraping and pelleted. Each cell pellet derived from one 15-cm dish was lysed in 1 ml of Lysis Buffer (LB) 1 solution [50 mM Hepes-KOH (pH 7.5), 140 mM NaCl, 1 mM EDTA, 10% glycerol, 0.5% NP-40, and 0.25% Triton X-100; all from Sigma-Aldrich] for 10 min on ice. The samples were centrifuged at 1350*g* for 5 min at 4°C. The resulting pellet was washed in 1 ml of LB2 solution [10 mM tris-HCl (pH 8), 200 mM NaCl, 1 mM EDTA, and 0.5 mM EGTA; all from Sigma-Aldrich] with gentle swirl 10 min at 4°C. Next, samples were centrifuged at 1350*g* for 5 min at 4°C, and the resulting pellet was lysed in 1 ml of LB3 solution [10 mM tris-HCl (pH 8), 100 mM NaCl, 1 mM EDTA, 0.5 mM EGTA, 0.1% Na-deoxycholate, and 0.5% *N*-lauroylsarcosine; all from Sigma-Aldrich]. LB1, LB2, and LB3 solutions were supplemented with protease inhibitor (cOmplete EDTA-free Protease Inhibitor Cocktail Tablets, Roche).

Chromatin isolated from both BAT and brown pre-adipocyte was sonicated with Bioruptor (Diagenode). Briefly, 1-ml aliquots of either WB3 or LB3 lysates in 15-ml polystyrene tubes were sonicated for two rounds of 10 min each (high intensity, 30 s on/30 s off). Before the precipitation step, Triton X-100 (Sigma-Aldrich) was added to chromatin samples at a final concentration of 1%. For both histone and histone modification, 5 µg of chromatin was diluted in a final volume of 1 ml in LB3 buffer and incubated with 5 µg of antibody overnight at 4°C in rotation. The equivalent of 10% of single IP was collected as input fraction. The day after, Dynabeads Protein G (Thermo Fisher Scientific) were washed three times with 0.5% BSA (Jackson ImmunoResearch) in PBS, and 50 µl of washed beads was added to each sample and rotated for 3 hours at 4°C. Then, five washes with radioimmunoprecipitation assay buffer [1 mM EDTA, 50 mM Hepes-KOH (pH 7.6), 500 mM LiCl, 1% NP-40, and 0.7% Na-deoxycholate; all from Sigma-Aldrich] and one wash with TE buffer [10 mM tris-HCl (pH 8) and 1 mM EDTA; both from Sigma-Aldrich] containing 50 mM NaCl were performed. Next, samples were centrifuged for 3 min at 960*g* at 4°C. The supernatant was discarded, and 250 µl of elution buffer (TE buffer with 2% SDS) was added to the beads-antibody-chromatin complex. Samples were incubated in a thermo mixer for 15 min at 65°C while shaking and then centrifuged for 1 min at room temperature at 16,360*g*. The supernatant was transferred to a new tube, and samples, together with the input fractions to which 170 µl of elution buffer was added (final volume, 250 µl), were cross-link–reverted overnight at 65°C. The day after, samples were incubated for 1 hour at 55°C with 5 µl of Proteinase K (stock, 20 mg/ml; Promega). For DNA purification, the QIAquick PCR Purification Kit was used (Qiagen), following the manufacturer's recommendations. DNA was eluted in 50 µl of TE buffer, and 1 µl was analyzed in quantitative real-time PCR with the SYBR GreenER qPCR Kit (Thermo Fisher Scientific). Antibodies and primers used for ChIP-qPCR analysis are listed in table S4.

RNA sequencing

Total RNA was extracted using RNA spin columns (PureLink RNA Mini Kit, Ambion). For RNA-seq Young (Fig. 3 and table S1), total RNA was extracted from control- and Suv420h dKO–derived BAT. For RNA-seq Diet (Fig. 5 and table S1), total RNA was isolated from BAT collected from control and Suv420h dKO mice in both diet regimens. RNA quantification was carried out using Qubit Fluorometric Quantification (Life Technologies), and 500 ng of RNA was used to prepare the library. Library generation was performed using the QuantSeq 3′ mRNA-seq Library Prep Kit. The procedure was initiated by oligo(dT) priming, and then the first-strand synthesis and RNA removal were followed by random-primed synthesis of the complementary strand. The resulting double-stranded cDNA was purified with magnetic beads to remove all reaction components. The adapter sequences were added by library PCR amplification, and the proper cycle number was previously determined by qPCR. The library was purified from PCR components using purification beads. Last, the quality of the samples was determined using Bioanalyzer (Agilent Technologies). Libraries were sequenced using an Illumina HiSeq 2500 System based on standard protocols (100-base-pair single-end reads). Raw sequencing reads (FASTQ) were processed individually and mapped to the mouse genome reference version GRCm38 (mm10) from Gencode (M13). The mapping was performed using STAR (v2.5.3a) (http://code.google.com/p/rna-star/) using soft clipping and all other parameters set to default values according to recommended data analysis workflow by Lexogen. Gene abundance was determined using featureCounts (http://subread.sourceforge.net) and normalized using calcNormFactors function from edgeR R/Bioconductor package (http://bioconductor.org) followed by differential gene expression analysis using limma (http://www.bioconductor.org) for differences due to the genotype (KO versus control). In RNA-seq Diet, the treatment (ND/HFD) was added as a covariate. Genes were considered as expressed when showing more than 1 cpm and differentially expressed when showing a false discovery rate (FDR) < 0.1. RNA-Seq data of both experiments have been uploaded to the Gene Expression Omnibus (GEO) database (https://www.ncbi.nlm.nih.gov/geo/), with accession number GSE117482.

Functional enrichment

For functional enrichment analyses, Enrichr web tool was used (http://amp.pharm.mssm.edu/Enrichr/). Briefly, Enrichr performs a Fisher enrichment test, corrects for multiple comparisons, and applies an additional *Z* score on *P* values to provide additional information on Fisher *P* value relevance (http://amp.pharm.mssm.edu/Enrichr/). Kyoto Encyclopedia of Genes and Genomes (KEGG), Biocarta, Reactome, and WikiPathways databases (2016) were used for pathway enrichment, and Gene Ontology biological processes, molecular function, and cellular components databases (2015) were used for ontologies. ChEA (ChIP-Seq enrichment experiments database, 2016) was used to explore enrichment in DNA binding factors. For pathway analysis (Figs. 3 and 5 and table S2), categories were considered enriched when shown an FDR < 0.05, a *Z* score < −1.75, and three or more genes in overlap.

ChEA of up-regulated targets in dKO mice, both in RNA-seq Young and in RNA-seq Diet, revealed that several PPAR-γ ChIP-Seq experiments were significantly enriched. Those results are cited and presented in table S3 under the sheet name "ChEA_Analysis (RNA-seq Young)" and "ChEA_Analysis (RNA-seq Diet)." Genes present in each of the datasets (DatasetID_PubMedID_ChIP-Seq_CellLine_Species) and up-regulated in both experiments are present under the first and second sheets of table S3 under the name "PPAR-g targets UP (RNA-seq Young)" and "PPAR-g targets UP (RNA-seq Diet)" with their respective log2FC and *P* value for dKO RNA-seq experiments.

We have defined a very comprehensive set of PPAR-γ targets as the union of all genes present in PPAR-γ ChIP experiments (ChEA_2016, ENCODE_and_ChEA_Consensus_TFs_from:ChIP-X), genes up-regulated after PPAR-γ perturbations (TF_Perturbations_Followd_by_Expression), genes up-regulated upon PPAR-γ agonist stimulation (Drug_Perturbations_from _GEO_up) and PPAR-γ overexpression (Single_Gene_Perturbations_from:GEO_up), and PPAR-γ signaling pathway genes (KEGG, WikiPathways) for RNA-seq Young that were separately found enriched by *Enrichr*. In the RNA-seq Diet, we also included those for the transcription factor coexpression database (ARCHS4_TFs_Coexp) and an internal database of Enrichr (Enrichr_Submissions_TF-Gene_Coocurrence) (table S3). GSEA preranked analysis was performed using the Java version of the software (gsea2–2.2.3.jar; software.broadinstitute.org/gsea/), using the log2FC-obtained RNA-seq contrasts (RNA-seq Young genotype and RNA-seq Diet genotype contrast).

To generate Figs. 3B and 5B and figs. S3 and S5, the significant categories were grouped in clusters based on a higher hierarchy of

biological processes or components after careful visual inspection. This clustering of categories contributes to enhance the interpretability of functional enrichment analyses. In the figures, a graph linking genes with each other when belonging to the same category was made using the R package FGNet (http://bioconductor.org/packages/release/bioc/html/FGNet.html), and the clusters of the different significant categories were made visible by grouping the genes together using Cytoscape (https://cytoscape.org/). For a few genes belonging to categories included in different clusters, the gene was manually placed into one unique cluster after careful inspection of its literature and deciding to which high hierarchy biological process it belongs.

Statistics

Unless stated otherwise, statistical comparisons were two-tailed tests and performed using GraphPad Prism 6 (GraphPad Software). The type of statistical test and the number of independent experiments are provided for each dataset in the corresponding figure legend. The differences were considered statistically significant when $P \leq 0.05$ and was reported as follows: $^{***}P \leq 0.001$, $^{**}P \leq 0.01$, $^{*}P \leq 0.05$.

SUPPLEMENTARY MATERIALS

Supplementary material for this article is available at http://advances.sciencemag.org/cgi/content/full/5/4/eaav1472/DC1

Fig. S1. Suv420h analysis in different metabolic tissues.
Fig. S2. Suv420h epigenetic mark decreases upon cold exposure.
Fig. S3. Validation of up-regulated genes and clustering of down-regulated genes for RNA-seq Young.
Fig. S4. Validation of up-regulated genes for RNA-seq Diet.
Fig. S5. Clustering of down-regulated genes for RNA-seq Diet.
Fig. S6. Overlap of differentially expressed genes in RNA-seq Young and RNA-seq Diet.
Data file S1. RNA-seq data analysis, RNA-seq Young, and RNA-seq Diet.
Data file S2. Functional enrichment analysis, RNA-seq Young, and RNA-seq Diet.
Data file S3. PPAR-γ targets up-regulated in KO versus control (RNA-seq Young and RNA-seq Diet).
Data file S4. List of primers and antibodies.

REFERENCES AND NOTES

1. S. Verma, M. E. Hussain, Obesity and diabetes: An update. *Diabetes Metab. Syndr.* **11**, 73–79 (2017).
2. K. Bhaskaran, I. Douglas, H. Forbes, I. dos-Santos-Silva, D. A. Leon, L. Smeeth, Body-mass index and risk of 22 specific cancers: A population-based cohort study of 5.24 million U.K. adults. *Lancet* **384**, 755–765 (2014).
3. S. J. van Dijk, R. L. Tellam, J. L. Morrison, B. S. Muhlhausler, P. L. Molloy, Recent developments on the role of epigenetics in obesity and metabolic disease. *Clin. Epigenetics* **7**, 66 (2015).
4. G.-X. Wang, X.-Y. Zhao, J. D. Lin, The brown fat secretome: Metabolic functions beyond thermogenesis. *Trends Endocrinol. Metab.* **26**, 231–237 (2015).
5. A. Vargas-Castillo, R. Fuentes-Romero, L. A. Rodriguez-Lopez, N. Torres, A. R. Tovar, Understanding the biology of thermogenic fat: Is browning a new approach to the treatment of obesity? *Arch. Med. Res.* **48**, 401–413 (2017).
6. M. P. B. Moonen, E. B. M. Nascimento, W. D. van Marken Lichtenbelt, Human brown adipose tissue: Underestimated target in metabolic disease? *Biochim. Biophys. Acta Mol. Cell. Biol. Lipids* **1864**, 104–112 (2019).
7. G. Weir, L. E. Ramage, M. Akyol, J. K. Rhodes, C. J. Kyle, A. M. Fletcher, T. H. Craven, S. J. Wakelin, A. J. Drake, M.-L. Gregoriades, C. Ashton, N. Weir, E. J. R. van Beek, F. Karpe, B. R. Walker, R. H. Stimson, Substantial metabolic activity of human brown adipose tissue during warm conditions and cold-induced lipolysis of local triglycerides. *Cell Metab.* **27**, 1348–1355.e4 (2018).
8. J. Wu, P. Boström, L. M. Sparks, L. Ye, J. H. Choi, A.-H. Giang, M. Khandekar, K. A. Virtanen, P. Nuutila, G. Schaart, K. Huang, H. Tu, W. D. van Marken Lichtenbelt, J. Hoeks, S. Enerbäck, P. Schrauwen, B. M. Spiegelman, Beige adipocytes are a distinct type of thermogenic fat cell in mouse and human. *Cell* **150**, 366–376 (2012).
9. M. Chondronikola, L. S. Sidossis, Brown and beige fat: From molecules to physiology. *Biochim. Biophys. Acta Mol. Cell. Biol. Lipids* **1864**, 91–103 (2019).
10. R. E. Soccio, Z. Li, E. R. Chen, Y. H. Foong, K. K. Benson, J. R. Dispirito, S. E. Mullican, M. J. Emmett, E. R. Briggs, L. C. Peed, R. K. Dzeng, C. J. Medina, J. F. Jolivert, M. Kissig, S. R. Rajapurkar, M. Damle, H.-W. Lim, K.-J. Won, P. Seale, D. J. Steger, M. A. Lazar, Targeting PPAR-γ in the epigenome rescues genetic metabolic defects in mice. *J. Clin. Invest.* **127**, 1451–1462 (2017).
11. C. Lapa, P. Arias-Loza, N. Hayakawa, H. Wakabayashi, R. A. Werner, X. Chen, T. Shinaji, K. Herrmann, T. Pelzer, T. Higuchi, Whitening and impaired glucose utilization of brown adipose tissue in a rat model of type 2 diabetes mellitus. *Sci. Rep.* **7**, 16795 (2017).
12. A. M. Sharma, B. Staels, Peroxisome proliferator-activated receptor-γ and adipose tissue—Understanding obesity-related changes in regulation of lipid and glucose metabolism. *J. Clin. Endocrinol. Metab.* **92**, 386–395 (2007).
13. S. G. Dubois, L. K. Heilbronn, S. R. Smith, J. B. Albu, D. E. Kelley, E. Ravussin; Look AHEAD Adipose Research Group, Decreased expression of adipogenic genes in obese subjects with type 2 diabetes. *Obesity* **14**, 1543–1552 (2006).
14. I. Barroso, M. Gurnell, V. E. F. Crowley, M. Agostini, J. W. Schwabe, M. A. Soos, G. L. Maslen, T. D. M. Williams, H. Lewis, A. J. Schafer, V. K. K. Chatterjee, S. O'Rahilly, Dominant negative mutations in human PPAR-γ associated with severe insulin resistance, diabetes mellitus and hypertension. *Nature* **402**, 880–883 (1999).
15. S. Sugii, P. Olson, D. D. Sears, M. Saberi, A. R. Atkins, G. D. Barish, S.-H. Hong, G. L. Castro, Y.-Q. Yin, M. C. Nelson, G. Hsiao, D. R. Greaves, M. Downes, R. T. Yu, J. M. Olefsky, R. M. Evans, PPAR-γ activation in adipocytes is sufficient for systemic insulin sensitization. *Proc. Natl. Acad. Sci. U.S.A.* **106**, 22504–22509 (2009).
16. S. Wang, E. J. Dougherty, R. L. Danner, PPAR-γ signaling and emerging opportunities for improved therapeutics. *Pharmacol. Res.* **111**, 76–85 (2016).
17. M. A. Lazar, Reversing the curse on PPARγ. *J. Clin. Invest.* **128**, 2202–2204 (2018).
18. M. J. Kraakman, Q. Liu, J. Postigo-Fernandez, R. Ji, N. Kon, D. Larrea, M. Namwanje, L. Fan, M. Chan, E. Area-Gomez, W. Fu, R. J. Creusot, L. Qiang, PPAR-γ deacetylation dissociates thiazolidinedione's metabolic benefits from its adverse effects. *J. Clin. Invest.* **128**, 2600–2612 (2018).
19. G. Schotta, M. Lachner, K. Sarma, A. Ebert, R. Sengupta, G. Reuter, D. Reinberg, T. Jenuwein, A silencing pathway to induce H3-K9 and H4-K20 trimethylation at constitutive heterochromatin. *Genes Dev.* **18**, 1251–1262 (2004).
20. G. Schotta, R. Sengupta, S. Kubicek, S. Malin, M. Kauer, E. Callén, A. Celeste, M. Pagani, S. Opravil, I. A. De La Rosa-Velazquez, A. Espejo, M. T. Bedford, A. Nussenzweig, M. Busslinger, T. Jenuwein, A chromatin-wide transition to H4K20 monomethylation impairs genome integrity and programmed DNA rearrangements in the mouse. *Genes Dev.* **22**, 2048–2061 (2008).
21. M. Hahn, S. Dambacher, S. Dulev, A. Y. Kuznetsova, S. Eck, S. Wörz, D. Sadic, M. Schulte, J.-P. Mallm, A. Maiser, P. Debs, H. von Melchner, H. Leonhardt, L. Schermelleh, K. Rohr, K. Rippe, Z. Storchova, G. Schotta, Suv4-20h2 mediates chromatin compaction and is important for cohesin recruitment to heterochromatin. *Genes Dev.* **27**, 859–872 (2013).
22. R. C. J. Twells, M. L. Metzker, S. D. Brown, R. Cox, C. Garey, H. Hammond, P. J. Hey, E. Levy, Y. Nakagawa, M. S. Philips, J. A. Todd, J. F. Hess, The sequence and gene characterization of a 400-kb candidate region for *IDDM4* on chromosome 11q13. *Genomics* **72**, 231–242 (2001).
23. V. Faundes, W. G. Newman, L. Bernardini, N. Canham, J. Clayton-Smith, B. Dallapiccola, S. J. Davies, M. K. Demos, A. Goldman, H. Gill, R. Horton, B. Kerr, D. Kumar, A. Lehman, S. McKee, J. Morton, M. J. Parker, J. Rankin, L. Robertson, I. K. Temple, S. Banka, S. Adam, C. du Souich, A. M. Elliott, A. Lehman, J. Mwenifumbo, T. N. Nelson, C. van Karnebeek, J. M. Friedman, J. F. McRae, S. Clayton, T. W. Fitzgerald, J. Kaplanis, E. Prigmore, D. Rajan, A. Sifrim, S. Aitken, N. Akawi, M. Alvi, K. Ambridge, D. M. Barrett, T. Bayzetinova, P. Jones, W. D. Jones, D. King, N. Krishnappa, L. E. Mason, T. Singh, A. R. Tivey, M. Ahmed, U. Anjum, H. Archer, R. Armstrong, J. Awada, M. Balasubramanian, S. Banka, D. Baralle, A. Barnicoat, P. Batstone, D. Baty, C. Bennett, J. Berg, B. Bernhard, A. P. Bevan, M. Bitner-Glindzicz, E. Blair, M. Blyth, D. Bohanna, L. Bourdon, D. Bourn, L. Bradley, A. Brady, S. Brent, C. Brewer, K. Brunstrom, D. J. Bunyan, J. Burn, N. Canham, B. Castle, K. Chandler, E. Chatzimichali, D. Cilliers, A. Clarke, S. Clasper, J. Clayton-Smith, V. Clowes, A. Coates, T. Cole, I. Colgiu, A. Collins, M. N. Collinson, F. Connell, N. Cooper, H. Cox, L. Cresswell, G. Cross, Y. Crow, M. D'Alessandro, T. Dabir, R. Davidson, S. Davies, D. de Vries, J. Dean, C. Deshpande, G. Devlin, A. Dixit, A. Dobbie, A. Donaldson, D. Donnai, D. Donnelly, C. Donnelly, A. Douglas, S. Douzgou, A. Duncan, J. Eason, S. Ellard, I. Ellis, F. Elmslie, K. Evans, S. Everest, T. Fendick, R. Fisher, F. Flinter, N. Foulds, A. Fry, A. Fryer, C. Gardiner, L. Gaunt, N. Ghali, R. Gibbons, H. Gill, J. Goodship, D. Goudie, E. Gray, A. Green, P. Greene, L. Greenhalgh, S. Gribble, R. Harrison, L. Harrison, V. Harrison, R. Hawkins, L. He, S. Hellens, A. Henderson, S. Hewitt, L. Hildyard, E. Hobson, S. Holden, M. Holder, S. Holder, G. Hollingsworth, T. Homfray, M. Humphreys, J. Hurst, B. Hutton, S. Ingram, M. Irving, L. Islam, A. Jackson, J. Jarvis, L. Jenkins, D. Johnson, E. Jones, D. Josifova, S. Joss, B. Kaemba, S. Kazembe, R. Kelsell, B. Kerr, H. Kingston, U. Kini, E. Kinning, G. Kirby, C. Kirk, E. Kivuva, A. Kraus, D. Kumar, V. K. A. Kumar, K. Lachlan, W. Lam, A. Lampe, C. Langman, M. Lees, D. Lim, C. Longman, G. Lowther, S. A. Lynch, A. Magee, E. Maher, A. Male, S. Mansour, K. Marks, K. Martin, U. Maye, E. McCann, V. McConnell, M. McEntagart,

R. McGowan, K. McKay, S. McKee, D. J. McMullan, S. McNerlan, C. McWilliam, S. Mehta, K. Metcalfe, A. Middleton, Z. Miedzybrodzka, E. Miles, S. Mohammed, T. Montgomery, D. Moore, S. Morgan, J. Morton, H. Mugalaasi, V. Murday, H. Murphy, S. Naik, A. Nemeth, L. Nevitt, R. Newbury-Ecob, A. Norman, R. O'Shea, C. Ogilvie, K. R. Ong, S. M. Park, M. J. Parker, C. Patel, J. Paterson, S. Payne, D. Perrett, J. Phipps, D. T. Pilz, M. Pollard, C. Pottinger, J. Poulton, N. Pratt, K. Prescott, S. Price, A. Pridham, A. Procter, H. Purnell, O. Quarrell, N. Ragge, R. Rahbari, J. Randall, J. Rankin, L. Raymond, D. Rice, L. Robert, E. Roberts, J. Roberts, P. Roberts, G. Roberts, A. Ross, E. Rosser, A. Saggar, S. Samant, J. Sampson, R. Sandford, A. Sarkar, S. Schweiger, R. Scott, I. Scurr, A. Selby, A. Seller, C. Sequeira, N. Shannon, S. Sharif, C. Shaw-Smith, E. Shearing, D. Shears, E. Sheridan, I. Simonic, R. Singzon, Z. Skitt, A. Smith, K. Smith, S. Smithson, L. Sneddon, M. Splitt, M. Squires, F. Stewart, H. Stewart, V. Straub, M. Suri, V. Sutton, G. J. Swaminathan, E. Sweeney, K. Tatton-Brown, C. Taylor, R. Taylor, M. Tein, I. K. Temple, J. Thomson, M. Tischkowitz, S. Tomkins, A. Torokwa, B. Treacy, C. Turner, P. Turnpenny, C. Tysoe, A. Vandersteen, V. Varghese, P. Vasudevan, P. Vijayarangakannan, J. Vogt, E. Wakeling, S. Wallwark, J. Waters, A. Weber, D. Wellesley, M. Whiteford, S. Widaa, S. Wilcox, E. Wilkinson, D. Williams, N. Williams, L. Wilson, G. Woods, C. Wragg, M. Wright, L. Yates, M. Yau, C. Nellåker, M. Parker, H. V. Firth, C. F. Wright, D. R. FitzPatrick, J. C. Barrett, M. E. Hurles, Histone lysine methylases and demethylases in the landscape of human developmental disorders. *Am. J. Hum. Genet.* **102**, 175–187 (2018).

24. Q. Zhong, R. A. Kowluru, Epigenetic changes in mitochondrial superoxide dismutase in the retina and the development of diabetic retinopathy. *Diabetes* **60**, 1304–1313 (2011).
25. S. B. Cassidy, S. Schwartz, J. L. Miller, D. J. Driscoll, Prader-Willi syndrome. *Genet. Med.* **14**, 10–26 (2012).
26. M.-Y. Wu, T. F. Tsai, A. L. Beaudet, Deficiency of *Rbbp1*/*Arid4a* and *Rbbp1l1*/*Arid4b* alters epigenetic modifications and suppresses an imprinting defect in the PWS/AS domain. *Genes Dev.* **20**, 2859–2870 (2006).
27. R. J. Miltenberger, R. L. Mynatt, J. E. Wilkinson, R. P. Woychik, The role of the *agouti* gene in the yellow obese syndrome. *J. Nutr.* **127**, 1902S–1907S (1997).
28. D. C. Dolinoy, J. R. Weidman, R. A. Waterland, R. L. Jirtle, Maternal genistein alters coat color and protects A^{vy} mouse offspring from obesity by modifying the fetal epigenome. *Environ. Health Perspect.* **114**, 567–572 (2006).
29. A. A. Hardikar, S. N. Satoor, M. S. Karandikar, M. V. Joglekar, A. S. Puranik, W. Wong, S. Kumar, A. Limaye, D. S. Bhat, A. S. Januszewski, M. R. Umrani, A. K. Ranjan, K. Apte, P. Yajnik, R. R. Bhonde, S. Galande, A. C. Keech, A. J. Jenkins, C. S. Yajnik, Multigenerational undernutrition increases susceptibility to obesity and diabetes that is not reversed after dietary recuperation. *Cell Metab.* **22**, 312–319 (2015).
30. C. M. Webster, L. Wu, D. Douglas, A. A. Soukas, A non-canonical role for the *C. elegans* dosage compensation complex in growth and metabolic regulation downstream of TOR complex 2. *Development* **140**, 3601–3612 (2013).
31. C.-M. Hung, C. M. Calejman, J. Sanchez-Gurmaches, H. Li, C. B. Clish, S. Hettmer, A. J. Wagers, D. A. Guertin, Rictor/mTORC2 loss in the *Myf5* lineage reprograms brown fat metabolism and protects mice against obesity and metabolic disease. *Cell Rep.* **8**, 256–271 (2014).
32. A. Öst, A. Lempradl, E. Casas, M. Weigert, T. Tiko, M. Deniz, L. Pantano, U. Boenisch, P. M. Itskov, M. Stoeckius, M. Ruf, N. Rajewsky, G. Reuter, N. Iovino, C. Ribeiro, M. Alenius, S. Heyne, T. Vavouri, J. A. Pospisilik, Paternal diet defines offspring chromatin state and intergenerational obesity. *Cell* **159**, 1352–1364 (2014).
33. J. Sanchez-Gurmaches, D. A. Guertin, Adipocytes arise from multiple lineages that are heterogeneously and dynamically distributed. *Nat. Commun.* **5**, 4099 (2014).
34. P. Seale, B. Bjork, W. Yang, S. Kajimura, S. Chin, S. Kuang, A. Scimè, S. Devarakonda, H. M. Conroe, H. Erdjument-Bromage, P. Tempst, M. A. Rudnicki, D. R. Beier, B. M. Spiegelman, PRDM16 controls a brown fat/skeletal muscle switch. *Nature* **454**, 961–967 (2008).
35. T. J. Schulz, P. Huang, T. L. Huang, R. Xue, L. E. McDougall, K. L. Townsend, A. M. Cypess, Y. Mishina, E. Gussoni, Y.-H. Tseng, Brown-fat paucity due to impaired BMP signalling induces compensatory browning of white fat. *Nature* **495**, 379–383 (2013).
36. N. Martinez-Lopez, D. Athonvarangkul, S. Sahu, L. Coletto, H. Zong, C. C. Bastie, J. E. Pessin, G. J. Schwartz, R. Singh, Autophagy in Myf5+ progenitors regulates energy and glucose homeostasis through control of brown fat and skeletal muscle development. *EMBO Rep.* **14**, 795–803 (2013).
37. M. J. Harms, J. Ishibashi, W. Wang, H.-W. Lim, S. Goyama, T. Sato, M. Kurokawa, K.-J. Won, P. Seale, Prdm16 is required for the maintenance of brown adipocyte identity and function in adult mice. *Cell Metab.* **19**, 593–604 (2014).
38. M. Kissig, J. Ishibashi, M. J. Harms, H.-W. Lim, R. R. Stine, K.-J. Won, P. Seale, PRDM16 represses the type I interferon response in adipocytes to promote mitochondrial and thermogenic programing. *EMBO J.* **36**, 1528–1542 (2017).
39. L. Zhuang, Y. Jang, Y.-K. Park, J.-E. Lee, S. Jain, E. Froimchuk, A. Broun, C. Liu, O. Gavrilova, K. Ge, Depletion of Nsd2-mediated histone H3K36 methylation impairs adipose tissue development and function. *Nat. Commun.* **9**, 1796 (2018).
40. M. A. Rudnicki, P. N. J. Schnegelsberg, R. H. Stead, T. Braun, H.-H. Arnold, R. Jaenisch, MyoD or Myf-5 is required for the formation of skeletal muscle. *Cell* **75**, 1351–1359 (1993).
41. L. Kassar-Duchossoy, B. Gayraud-Morel, D. Gomès, D. Rocancourt, M. Buckingham, V. Shinin, S. Tajbakhsh, Mrf4 determines skeletal muscle identity in Myf5:Myod double-mutant mice. *Nature* **431**, 466–471 (2004).
42. M. Yamamoto, N. P. Legendre, A. A. Biswas, A. Lawton, S. Yamamoto, S. Tajbakhsh, G. Kardon, D. J. Goldhamer, Loss of MyoD and Myf5 in skeletal muscle stem cells results in altered myogenic programming and failed regeneration. *Stem Cell Rep.* **10**, 956–969 (2018).
43. P. Seale, Transcriptional regulatory circuits controlling brown fat development and activation. *Diabetes* **64**, 2369–2375 (2015).
44. A. Bartelt, S. B. Widenmaier, C. Schlein, K. Johann, R. L. S. Goncalves, K. Eguchi, A. W. Fischer, G. Parlakgül, N. A. Snyder, T. B. Nguyen, O. T. Bruns, D. Franke, M. G. Bawendi, M. D. Lynes, L. O. Leiria, Y.-H. Tseng, K. E. Inouye, A. P. Arruda, G. S. Hotamisligil, Brown adipose tissue thermogenic adaptation requires Nrf1-mediated proteasomal activity. *Nat. Med.* **24**, 292–303 (2018).
45. P. Giesbertz, H. Daniel, Branched chain amino acids as biomarkers in diabetes. *Curr. Opin. Clin. Nutr. Metab. Care* **19**, 48–54 (2016).
46. G. Chinetti-Gbaguidi, M. A. Bouhlel, C. Copin, C. Duhem, B. Derudas, B. Neve, B. Noel, J. Eeckhoute, P. Lefebvre, J. R. Seckl, B. Staels, Peroxisome proliferator-activated receptor-γ activation induces 11β-hydroxysteroid dehydrogenase type 1 activity in human alternative macrophages. *Arterioscler. Thromb. Vasc. Biol.* **32**, 677–685 (2012).
47. K. D. Bromberg, T. R. H. Mitchell, A. K. Upadhyay, C. G. Jakob, M. A. Jhala, K. M. Comess, L. M. Lasko, C. Li, C. T. Tuzon, Y. Dai, F. Li, M. S. Eram, A. Nuber, N. B. Soni, V. Manaves, M. A. Algire, R. F. Sweis, M. Torrent, G. Schotta, C. Sun, M. R. Michaelides, A. R. Shoemaker, C. H. Arrowsmith, P. J. Brown, V. Santhakumar, A. Martin, J. C. Rice, G. G. Chiang, M. Vedadi, D. Barsyte-Lovejoy, W. N. Pappano, The SUV4-20 inhibitor A-196 verifies a role for epigenetics in genomic integrity. *Nat. Chem. Biol.* **13**, 317–324 (2017).
48. J. A. Martínez, F. I. Milagro, K. J. Claycombe, K. L. Schalinske, Epigenetics in adipose tissue, obesity, weight loss, and diabetes. *Adv. Nutr.* **5**, 71–81 (2014).
49. G. Egger, G. Liang, A. Aparicio, P. A. Jones, Epigenetics in human disease and prospects for epigenetic therapy. *Nature* **429**, 457–463 (2004).
50. M. Ahmadian, J. M. Suh, N. Hah, C. Liddle, A. R. Atkins, M. Downes, R. M. Evans, PPAR-γ signaling and metabolism: The good, the bad and the future. *Nat. Med.* **19**, 557–566 (2013).
51. A. Abbas, J. Blandon, J. Rude, A. Elfar, D. Mukherjee, PPAR-γ agonist in treatment of diabetes: Cardiovascular safety considerations. *Cardiovasc. Hematol. Agents Med. Chem.* **10**, 124–134 (2012).
52. M. Lehrke, M. A. Lazar, The many faces of PPAR-γ. *Cell* **123**, 993–999 (2005).
53. R. E. Soccio, E. R. Chen, M. A. Lazar, Thiazolidinediones and the promise of insulin sensitization in type 2 diabetes. *Cell Metab.* **20**, 573–591 (2014).
54. Y. Guan, C. Hao, D. R. Cha, R. Rao, W. Lu, D. E. Kohan, M. A. Magnuson, R. Redha, Y. Zhang, M. D. Breyer, Thiazolidinediones expand body fluid volume through PPAR-γ stimulation of ENaC-mediated renal salt absorption. *Nat. Med.* **11**, 861–866 (2005).
55. H. Zhang, A. Zhang, D. E. Kohan, R. D. Nelson, F. J. Gonzalez, T. Yang, Collecting duct-specific deletion of peroxisome proliferator-activated receptor-γ blocks thiazolidinedione-induced fluid retention. *Proc. Natl. Acad. Sci. U.S.A.* **102**, 9406–9411 (2005).
56. T. E. Akiyama, G. E. Skelhorne-Gross, E. D. Lightbody, R. E. Rubino, J. Y. Shi, L. A. McNamara, N. Sharma, E. I. Zycband, F. J. Gonzalez, H. Liu, J. W. Woods, C. H. Chang, J. P. Berger, C. J. B. Nicol, Endothelial cell–targeted deletion of PPAR-γ blocks rosiglitazone-induced plasma volume expansion and vascular remodeling in adipose tissue. *J. Pharmacol. Exp. Ther.* **368**, 514–523 (2019).
57. M. G. Myers Jr., C. F. Burant, PPAR-γ action: It's all in your head. *Nat. Med.* **17**, 544–545 (2011).
58. R. G. Walton, B. Zhu, R. Unal, M. Spencer, M. Sunkara, A. J. Morris, R. Charnigo, W. S. Katz, A. Daugherty, D. A. Howatt, P. A. Kern, B. S. Finlin, Increasing adipocyte lipoprotein lipase improves glucose metabolism in high fat diet-induced obesity. *J. Biol. Chem.* **290**, 11547–11556 (2015).
59. X. Hui, W. Zhu, Y. Wang, K. S. L. Lam, J. Zhang, D. Wu, E. W. Kraegen, Y. Li, A. Xu, Major urinary protein-1 increases energy expenditure and improves glucose intolerance through enhancing mitochondrial function in skeletal muscle of diabetic mice. *J. Biol. Chem.* **284**, 14050–14057 (2009).
60. E. Hinoi, Y. Nakamura, S. Takada, H. Fujita, T. Iezaki, S. Hashizume, S. Takahashi, Y. Odaka, T. Watanabe, Y. Yoneda, Growth differentiation factor-5 promotes brown adipogenesis in systemic energy expenditure. *Diabetes* **63**, 162–175 (2014).
61. H. C. Roh, L. T. Y. Tsai, M. Shao, D. Tenen, Y. Shen, M. Kumari, A. Lyubetskaya, C. Jacobs, B. Dawes, R. K. Gupta, E. D. Rosen, Warming induces significant reprogramming of beige, but not brown, adipocyte cellular identity. *Cell Metab.* **27**, 1121–1137.e5 (2018).
62. M. V. Neguembor, A. Xynos, M. C. Onorati, R. Caccia, S. Bortolanza, C. Godio, M. Pistoni, D. F. Corona, G. Schotta, D. Gabellini, FSHD muscular dystrophy region gene 1 binds

Suv4-20h1 histone methyltransferase and impairs myogenesis. *J. Mol. Cell Biol.* **5**, 294–307 (2013).
63. T. Touvier, C. De Palma, E. Rigamonti, A. Scagliola, E. Incerti, L. Mazelin, J.-L. Thomas, M. D'Antonio, L. Politi, L. Schaeffer, E. Clementi, S. Brunelli, Muscle-specific Drp1 overexpression impairs skeletal muscle growth via translational attenuation. *Cell Death Dis.* **6**, e1663 (2015).
64. S. Pambianco, M. Giovarelli, C. Perrotta, S. Zecchini, D. Cervia, I. Di Renzo, C. Moscheni, M. Ripolone, R. Violano, M. Moggio, M. T. Bassi, P. L. Puri, L. Latella, E. Clementi, C. De Palma, Reversal of defective mitochondrial biogenesis in limb-girdle muscular dystrophy 2D by independent modulation of histone and PGC-1α acetylation. *Cell Rep.* **17**, 3010–3023 (2016).

Acknowledgments: We are grateful to A. Boletta and G. Tonon for insightful suggestions. We thank P. Seale for the gift of the immortalized brown pre-adipocytes. **Funding:** Work in the Gabellini laboratory was supported by the Italian Epigenomics Flagship Project (EPIGEN), the FSHD Global Research Foundation, the ERA-Net for Research on Rare Diseases, the FSH Society, the Italian Ministry of Health, and the Italian Association for Cancer Research (AIRC under IG 2017—ID 19919). S.P. was supported by a Marie Curie Individual Fellowship (EASY-746974). This work was also supported by the Italian Ministry of Health with 5 × 1000 funds. Funding bodies had no role in the design of the study; in the collection, analysis, and interpretation of data; and in the writing of the manuscript. **Author contributions:** S.P. designed research studies, conducted experiments, acquired data, analyzed data, and wrote the manuscript; R.C. conducted experiments, acquired data, and analyzed data; M.V.N. designed research studies, conducted experiments, acquired data, and analyzed data; G.F. conducted experiments, acquired data, and analyzed data; J.M.G.-M. acquired and analyzed data; C.d.P. conducted experiments, acquired data, and analyzed data; T.C. conducted experiments, acquired data, and analyzed data; M.G. conducted experiments, acquired data, and analyzed data; P.M. conducted experiments, acquired data, and analyzed data; A.F. processed tissues for histology; I.M. acquired and analyzed data; M.R. designed research studies; F.S. and C.D. analyzed data; A.E. and E.C. designed research studies; and D.G. designed research studies, analyzed data, and wrote the manuscript. **Competing interests:** The authors declare that they have no competing interests. **Data and materials availability:** All data needed to evaluate the conclusions in the paper are present in the paper and/or the Supplementary Materials. Additional data related to this paper may be requested from the authors.

Submitted 24 August 2018
Accepted 28 February 2019
Published 17 April 2019
10.1126/sciadv.aav1472

Citation: S. Pedrotti, R. Caccia, M. V. Neguembor, J. M. Garcia-Manteiga, G. Ferri, C. de Palma, T. Canu, M. Giovarelli, P. Marra, A. Fiocchi, I. Molineris, M. Raso, F. Sanvito, C. Doglioni, A. Esposito, E. Clementi, D. Gabellini, The Suv420h histone methyltransferases regulate PPAR-γ and energy expenditure in response to environmental stimuli. *Sci. Adv.* **5**, eaav1472 (2019).